Photoreaction Boosting Phosphorescence Cascade Energy Transfer Based on Cucurbit[8]Uril Biaxial Polypseudorotaxane

Wen-Wen Xing, Hui-Juan Wang, Zhixue Liu, Zhen-Hai Yu, Heng-Yi Zhang,* and Yu Liu*

Cascade energy capturers based on supramolecular assembly have recently generated great research interest in the field of luminescent materials. Herein is reported a cucurbit[8]uril (CB[8])-encapsulated coumarin-bridged phenylpyridinium salt (G) to form biaxial polypseudorotaxane (G⊂CB[8]), which not only induces the phosphorescence of the guest G, but also activates the photodimerization of coumarin functional group in the CB[8] cavity (G-dimer⊂CB[8]) to further boost its phosphorescence emission, extending the phosphorescence lifetime from 271.3 to 430.3 μs and the quantum yield from 5.1% to 25.7% in aqueous solution. After co-assembly with amphiphilic calixarene (SC4AD), the supramolecular biaxial polypseudorotaxane G-dimer⊂CB[8] is changed to the nanoparticle. Compared with the alone G-dimer⊂CB[8], the phosphorescence intensity of G-dimer⊂CB[8]@SC4AD is significantly enhanced with the phosphorescence lifetime extending to 2.11 ms. Subsequently, by doping commercial dye rhodamine B (RhB) in the G-dimer⊂CB[8]@SC4AD assembly, an ultrahighly efficient phosphorescence-harvesting energy transfer process occurs with an energy transfer efficiency (Φ_{ET}) of 72.3% and an antenna effect of 396.8. Furthermore, the cascaded room temperature phosphorescence harvesting system is constructed via introducing the secondary near-infrared (NIR) acceptors Nile blue or Cy5 in the G-dimer⊂CB[8]@SC4AD:RhB system, which possesses a good biocompatibility and is successfully applied to NIR delayed fluorescence targeted imaging in HeLa cell.

1. Introduction

Constructing supramolecular phosphorescence cascade capturer has attracted much attention because the purely organic room temperature phosphorescence (RTP) possesses large Stokes shift, long lifetime,[1] and occurrence of cascade energy transfer from triplet states of phosphors to singlet states of dyes,[2] which has been successfully applied to photocatalysis[3] information security and anti-counterfeiting,[4] and biological imaging.[5] Although many researches have been carried out on the purely organic RTP cascade light-harvesting systems, the construction of these systems with long life time and high quantum yield in aqueous solutions still faces great challenges because of the strong quenching effect of water on excited state of luminescent materials and the free molecular motion during non-radiative decay,[6] thereby inevitably limiting their practical biological applications. Nowadays, methods of constructing the purely organic RTP materials are mainly divided into doping,[7] crystalline packing,[8] polymerization,[9] matrix rigidification,[10] host–guest interactions[11] and so on, in which supramolecular methodology based on host–guest complexation[12] has been proven to be an accessible method to obtain phosphorescence both in water and the solid phase. Recently, bromophenylpyridine, quinoline, or phthalimide derivatives with strong RTP confined by macrocycle cucurbit[n] urils (CB[n]s) were reported,[13] and further assembled into highly efficient phosphorescence energy transfer (PET) systems, which provides a strategy to construct materials with long lifetime near-infrared (NIR) emission. George and coworkers reported a highly effective RTP harvesting system by loading the phthalimide derivatives on the soluble inorganic silicate template to realize delayed fluorescence.[14] We reported purely organic RTP with a lifetime of 1.13 ms in aqueous solution through the secondary assembly of dibromophthalimide derivative, CB[7], and amphiphilic calixarene (SC4AD), and successfully constructed an effective cascade light-harvesting system.[15] In the process of constructing supramolecular phosphorescent materials, the photoreaction presented positive effects such as the anthrancene-modified bromophenylpyridine confined by CB[8] showing excellent organelle identification triggered by photo-oxidation.[16] It is well known that coumarin is a kind of fluorescent molecule with aromatic lactone and double bond

W.-W. Xing, H.-J. Wang, Z. Liu, Z.-H. Yu, H.-Y. Zhang, Y. Liu
College of Chemistry
State Key Laboratory of Elemento-Organic Chemistry
Nankai University
Tianjin 300071, P. R. China
E-mail: hyzhang@nankai.edu.cn; yuliu@nankai.edu.cn
Y. Liu
Collaborative Innovation Center of Chemical Science and Engineering
Tianjin 300071, P. R. China

The ORCID identification number(s) for the author(s) of this article can be found under https://doi.org/10.1002/adom.202202588.

structure and showed good photodimerization ability[17] which can be used as an efficient element to construct photo-responsive supramolecular system. However, supramolecular biaxial polypseudorotaxane with phosphorescence constructed by the photoreaction of coumarin hasn't been reported yet.

Herein, we reported a photodimerization-enhanced, long lifetime and highly efficient cascade phosphorescent light-harvesting system with delayed NIR emission constructed by coumarin modified phenyl pyridine salt (G), CB[8], SC4AD, and commercial dyes. First, G was bonded with CB[8] to construct polypseudorotaxane (G⊂CB[8]), inducing phosphorescent emission at 520 nm. Further irradiation by 365 nm light, the coumarin moiety in G occurred photodimerization and formed new polypseudorotaxane (G-dimer⊂CB[8]) leading to the quantum yield increased from 5.1% to 25.7%. Then SC4AD was added to the two polypseudorotaxanes for secondary assembly to enhance phosphorescent emission, leading to an ultralong lifetime RTP of 2.89 and 2.11 ms in aqueous solution, respectively. Benefiting from the excellent luminescent behaviors of the above two RTP systems, commercial dye rhodamine B (RhB) was introduced as the first donor to construct two phosphorescent light capture systems. Interestingly, G-dimer⊂CB[8]@SC4AD exhibited better energy transfer effect than the system that did not go through photodimerization process. Finally, G-dimer⊂CB[8]@SC4AD was selected to construct cascade phosphorescence-harvesting system and was successfully applied to delayed fluorescence-targeted cell imaging (**Scheme 1**). To the best of our knowledge, such a photodimerization-enhanced RTP biaxial polypseudorotaxane based on coumarin has not been reported before.

2. Results and Discussion

In this work, a water-soluble guest G was synthesized and characterized (Figures S1–S3, Supporting Information). First, the UV absorption spectrum and fluorescence emission spectrum of G were measured. The results showed that its maximum absorption occurred at 310 nm and the fluorescence emission at 390 nm (Figure S4, Supporting Information), respectively. As a control experiment, the absorption and emission spectra of coumarin functional group (M) and pyridine salt functional group (N) were measured, respectively (Figure S4, Supporting Information). CB[8] is competent to accommodate two hetero- or homo-guests simultaneously due to its large cavity,[18] forming complexes with a high binding constant. Job plot determined by UV absorption spectra showed a minimum value at $X_G = 0.5$, which preliminarily indicated that G was wrapped by CB[8] in a ratio of 1:1 (Figure S5, Supporting Information). Next, ^{1}H NMR, 2D NMR, and spectroscopic experiments were conducted to study the inclusion pattern of the assembly. ^{1}H NMR titration experiments demonstrated that the proton signals of G shifted toward higher field with the addition of CB[8], implying the coumarin and the pyridine salt moiety were contained in the cavity of CB[8] (**Figure 1** and Figure S9, Supporting Information). Furthermore, 2D rotating-frame Overhauser effect spectroscopy (ROESY) of G⊂CB[8] shows clear NOE cross-peaks between the coumarin's H_{10} and H_{11}, and the proton H_3 with H_1 of phenylpyridinium salt. These

observations indicate the formation of homologous inclusion complexes (Figure S10, Supporting Information). In order to further prove the "head to head" linear mode, diffusion-ordered spectroscopy experiments were carried out. The data indicated that the diffusion coefficients (*D*) of G and G⊂CB[8] were 4.7997×10^{-10} and 2.7766×10^{-10} m^2 s^{-1} (Figure S11, Supporting Information), respectively. On the basis of the Stokes–Einstein relationship, *D* and the radius of a spherical particle were not inversely proportional, suggesting the formation of supramolecular polypseudorotaxane. In addition, the fluorescence peak of G at 390 nm decreased and a new peak appeared at 520 nm with the gradual addition of CB[8] (**Figure 2**b), proving the formation of assembly G⊂CB[8]. When data at 390 nm in the fluorescence spectra were chosen to fit the binding constant (K_s), the K_s value obtained between G and CB[8] is 1.49×10^7 M^{-1} (Figure S6, Supporting Information). As exhibited in the 1931 CIE chromaticity diagram, with the gradual dripping of CB[8], the system moved from the purple luminous area to the green luminous area (Figure S12, Supporting Information). To confirm the property of the emerging peak located at 520 nm, transient spectra (delayed 0.1 ms) was measured. The results witnessed a continuous increasing of the emission at 520 nm during the process of drip addition, and it was also proved to be long-life (Figure 2c). Then, a large amount of nitrogen was pumped into the solution to exhaust the oxygen in the solution, and caused a significantly increase (Figure 2d). Meanwhile, on the grounds of the time-resolved photoluminescence (PL) decay curve (Figure 2f), the lifetime of 520 nm was measured to be 271.3 µs, so it was confirmed to be a phosphorescent emission peak. These results indicated that singlet electrons could be efficiently converted into long-lived triplet states. The reason why the encapsulation of G in CB[8] resulted in the RTP emission at 520 nm was that the macrocyclic encapsulation effectively inhibits the non-radiative transition caused by the disorder molecular motion and oxygen or other quenchers in water.[19] The above results were in well agreement with the "linear supramolecular polypseudorotaxane" strategy recently reported by us.[20] Therefore, we confirmed that the inclusion complexation between CB[8] and G can lead to the formation of linear supramolecular polypseudorotaxane in aqueous solution. Next, cucurbit[7]uril (CB[7]) with a smaller cavity was used as a host reference molecule to study its binding mode and optical behaviors with G. As shown in Figure S13, Supporting Information, the Job plot reaches a maximum at 0.67, which means that the binding stoichiometry is 1:2 between G and CB[7]. The high-resolution mass spectrometry also attested the conclusion (Figure S14, Supporting Information). The absorbance spectra showed a slight shift toward long wavelengths (Figure S15, Supporting Information) and the data at 280 nm were taken to fit the binding constants, and given the binding constants between CB[7] and G were 2.04×10^8 and 2.47×10^8 M^{-1}, respectively (Figure S16, Supporting Information). Moreover, fluorescence titration experiments showed that CB[7] could induce enhanced fluorescence intensity at 390 nm (Figure S17, Supporting Information). The fact of no new peak appearing, further indicated that only CB[8] can induce efficient phosphorescent emission of pyridine salt.

In order to make a deep research of the RTP behaviors of G⊂CB[8], amphiphilic calixarene (SC4AD) was introduced
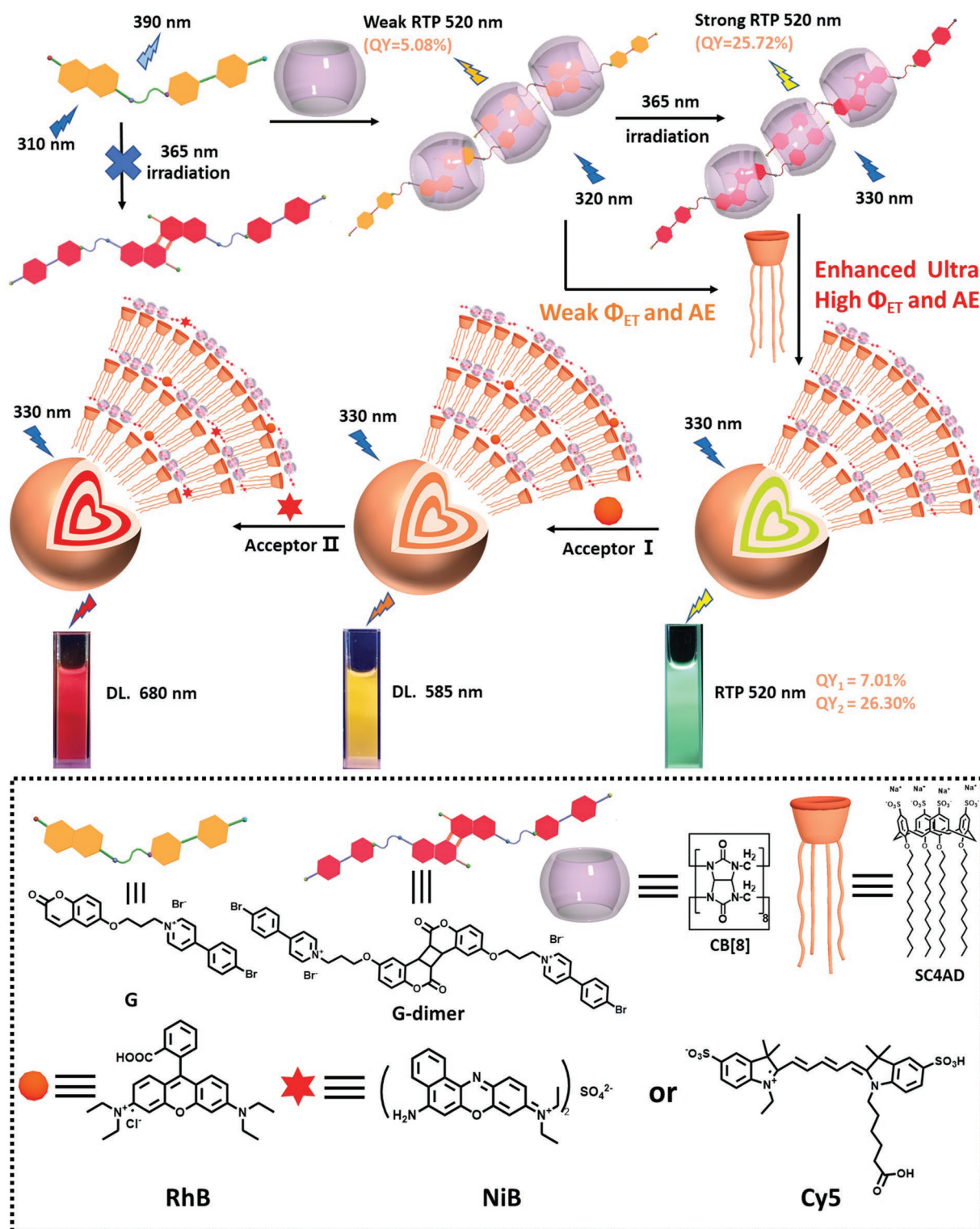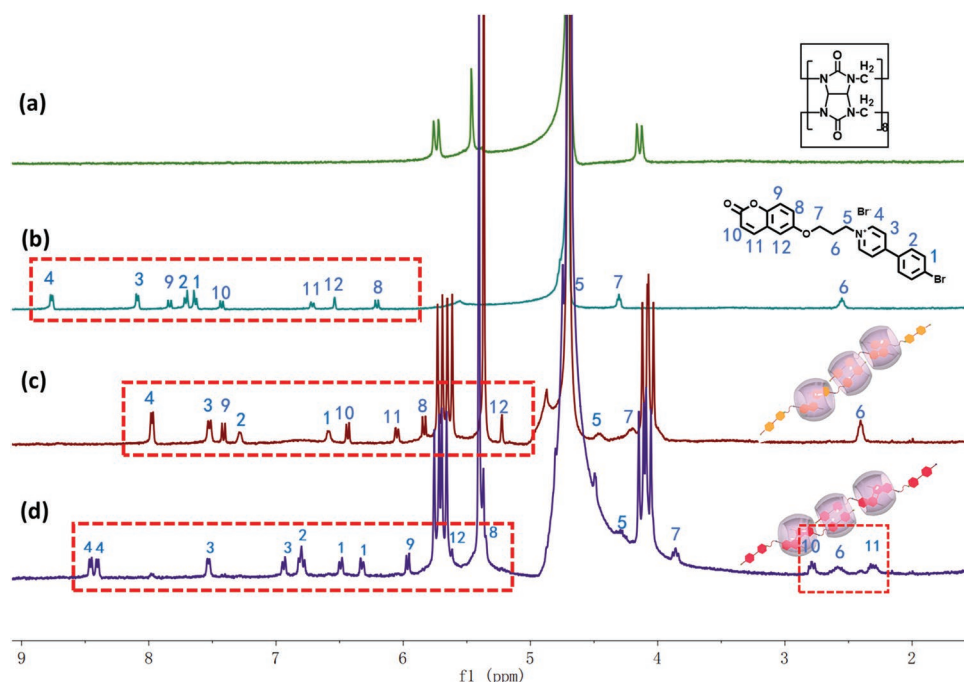
Scheme 1. Schematic illustration of a photodimerization-enhanced secondary purely organic RTP capture system.

and caused an obvious enhancement of the phosphorescence intensity at 520 nm. With the gradual addition of SC4AD from 1.5×10^{-6} to 7.5×10^{-6} M, the phosphorescence intensity at 520 nm keeps increasing and reaches maximum

(2.3-fold) (Figure 2e). The intensity of phosphorescence emission increases markedly because the construction of tertiary assembly further inhibits the non-radiative transition. Supramolecular assembly was formed by the electrostatic interactions
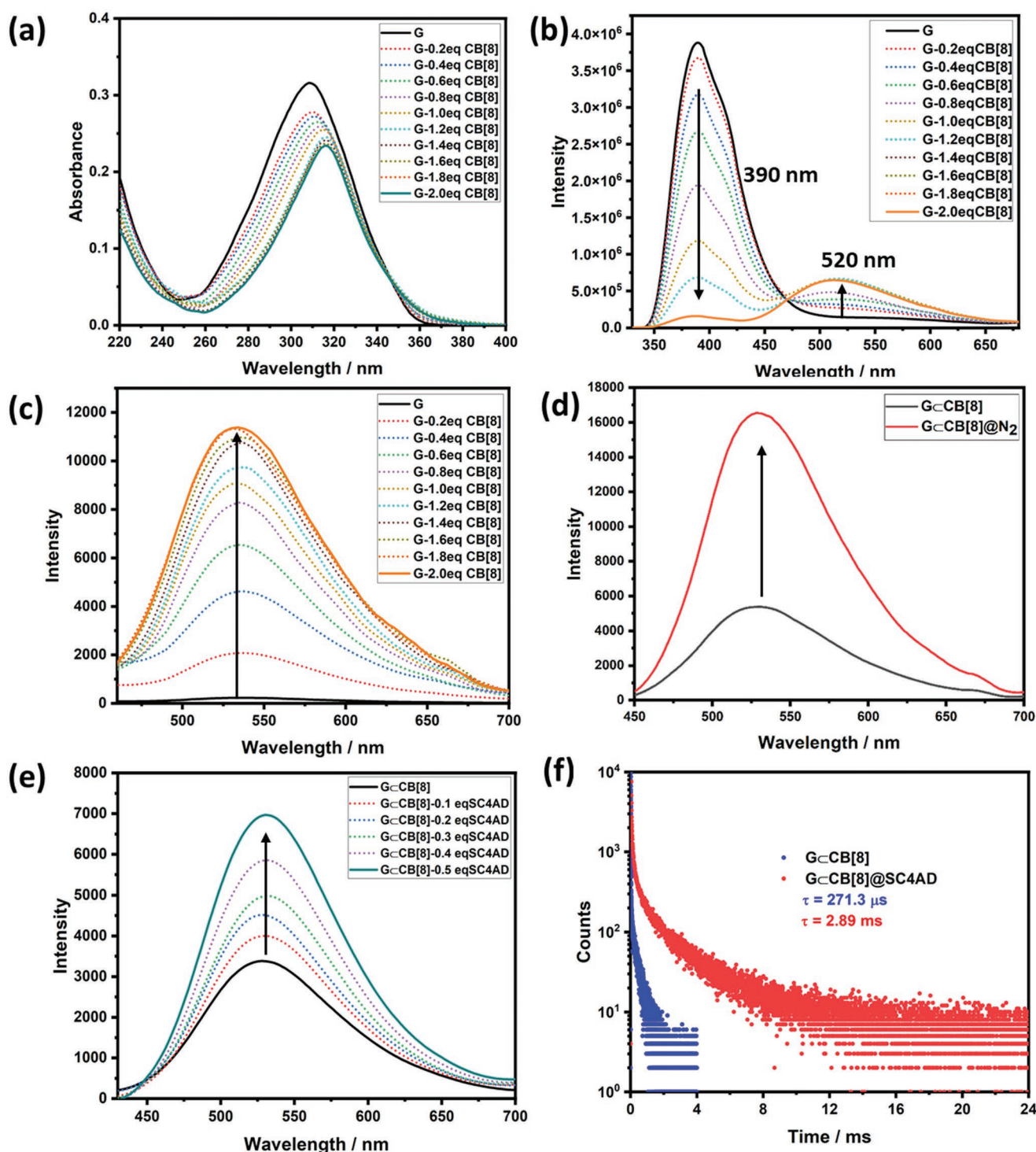
**ADVANCED
SCIENCE NEWS**
www.advancedsciencenews.com

**ADVANCED
OPTICAL
MATERIALS**
www.advopticalmat.de

Figure 1. ^{1}H NMR spectra of a) CB[8], b) G, c) G⊂CB[8], and d) G-dimer⊂CB[8] ([G] = [CB[8]] = 1 mм, 400 MHz, D$_2$O).

between the positive charge of G⊂CB[8] (or G-dimer⊂CB[8]) and the negative charge of SC4AD with the hydrophobic parts inside and hydrophilic parts outside, which caused the formation of nanospheres. On the other hand, the long alkyl chain of SC4AD has an excellent hydrophobic effect, which could prevent the quenching of the excited state of the luminescence body by water. Corresponding to the above results, the lifetime of the assembly G⊂CB[8]@SC4AD was fit for 2.89 ms (Figure 2f), which shows a significant increasing than that of G⊂CB[8]. Next, the zeta potential of G⊂CB[8]@SC4AD was measured and calculated as −51.37 mV (Figure S18, Supporting Information). Transmission electron microscopy (TEM) provides a visualization of G⊂CB[8]@SC4AD showing that the size of the supramolecular nanoparticles is around 150 nm (Figure S28, Supporting Information). Dynamic light scattering (DLS) experiments were measured to further prove the formation of nanoparticles. DLS data reveals that the average particle size of the nanospheres is about 121.13 nm, which is consistent with the TEM result (Figure S18, Supporting Information).

Noteworthily, possessing the excellent phosphorescence behavior of G⊂CB[8]@SC4AD, a light capturing system was expected to construct. Some commercial fluorescent dyes could be well loaded into the hydrophobic part and easily encapsulated into a tightly aligned G⊂CB[8]@SC4AD by the hydrophobic effect. At the same time, this also created the conditions for the short distance requirement between donor and acceptor. On the other hand, considering that the absorption spectrum of RhB can overlap well with the emission spectrum of G⊂CB[8]@SC4AD (Figure S19, Supporting Information), it is feasible to realize PET between them. As RhB was added to G⊂CB[8]@SC4AD gradually, the phosphorescence peak at 520 nm decreased continuously, while the peak at 585 nm appeared and increased continuously (**Figure 3**a). It was worth

noting that the emission peak of RhB could be clearly observed when the donor–acceptor ratio is only 4500:1. When the ratio of donor to recipient reached 100:1, Φ_{ET} was calculated as 48.62 (Figure S20, Supporting Information) and the antenna effect (AE) value could reach 274.89 (Figure S21, Supporting Information, and Figure 3b). The emission peak of the system was located at 585 nm which was the same as the position of the fluorescence emission peak of RhB, which could be concluded that the donor of triplet state energy can effectively transfer to the singlet state to achieve phosphorescent energy transfer. In accordance with the time-resolved curve, the lifetime of G⊂CB[8]@SC4AD:RhB at 520 and 585 nm was fitted as 145.5 and 285.5 μs, respectively (Figure 3e), which was consistent with the occurrence of PET and also provided favorable evidence for the transfer of donor energy from the triplet state to the singlet state of the acceptor.

Afterward, the properties of G⊂CB[8] assembly under UV irradiation were investigated. First, assembly G⊂CB[8] witnessed a significant increase of phosphorescence emission peak at 520 nm in the steady-state spectrum with the irradiation of 365 nm light (**Figure 4**a and Figure S22, Supporting Information), while the fluorescence peak at 390 nm is almost unchanged. Thus, it could be preliminarily inferred that the coumarin of G undergoes photodimerization under UV light irradiation, which leads to the change of assembly structure. Moreover, the corresponding phosphorescence spectra (delayed 0.1 ms) were tested and the results are consistent with those mentioned above (Figure 4b). As shown in Figure 4c and Figure S23, Supporting Information, both the life-time and the quantum yield of the system after illumination have been improved to some extent, in which, the lifetime increased from 271.1 to 430.3 μs, and the quantum yield significantly increases from 5.1% to 25.7%. In order to verify whether the change of

**ADVANCED
SCIENCE NEWS**

www.advancedsciencenews.com

**ADVANCED
OPTICAL
MATERIALS**

www.advopticalmat.de

Figure 2. a) UV–vis absorption spectra, b) photoluminescence spectra, and c) phosphorescence spectra (delayed 0.1 ms) changes of G (0.01 mм) upon gradual addition of CB[8] ranging from 0 to 0.02 mм (λ_{ex} = 320 nm). d) Phosphorescence spectra (delayed 0.1 ms) of G⊂CB[8] and G⊂CB[8]@ N_2, ([G] = 0.015 mм, [CB[8]] = 0.03 mм). e) Phosphorescence spectra (delayed 0.1 ms) of G⊂CB[8] with increasing concentration of SC4AD. f) The time-resolved PL decay curve of G⊂CB[8] and G⊂CB[8]@SC4AD at 520 nm ([G] = [CB[8]] = 0.01 mм, λ_{ex} = 320 nm).

phosphorescence intensity was caused by photodimerization of coumarin, the ^{1}H NMR titration experiments with the irradiation of light of assembly G⊂CB[8] were carried out. As depicted in Figure S24, Supporting Information, with the extension

of illumination time, protons of the guest molecule had an overall trend of moving toward high fields. Further integration shows that the hydrogen of the double bond shifts to 2.3–2.8, which fully prove that coumarin in the assembly do form a
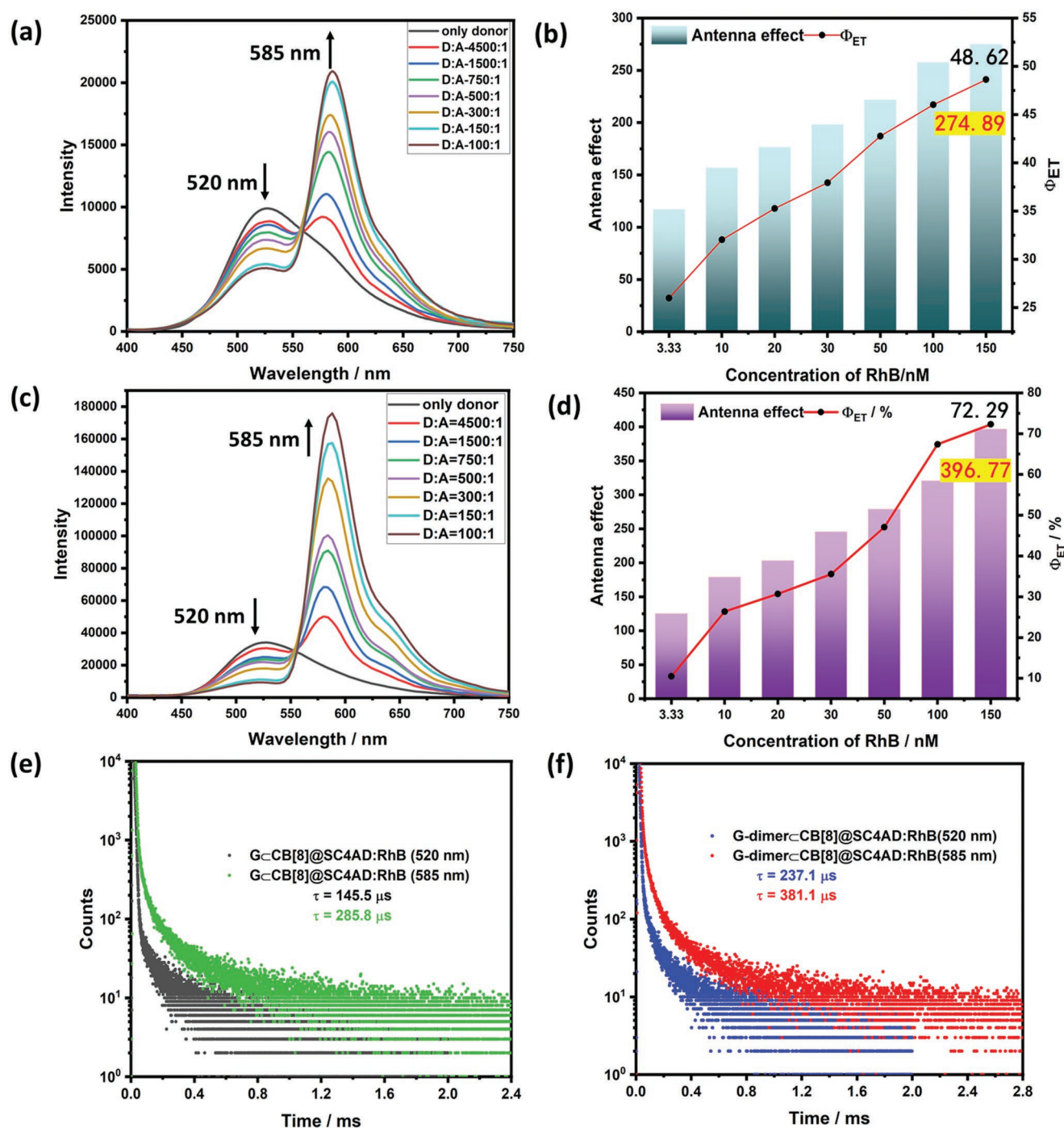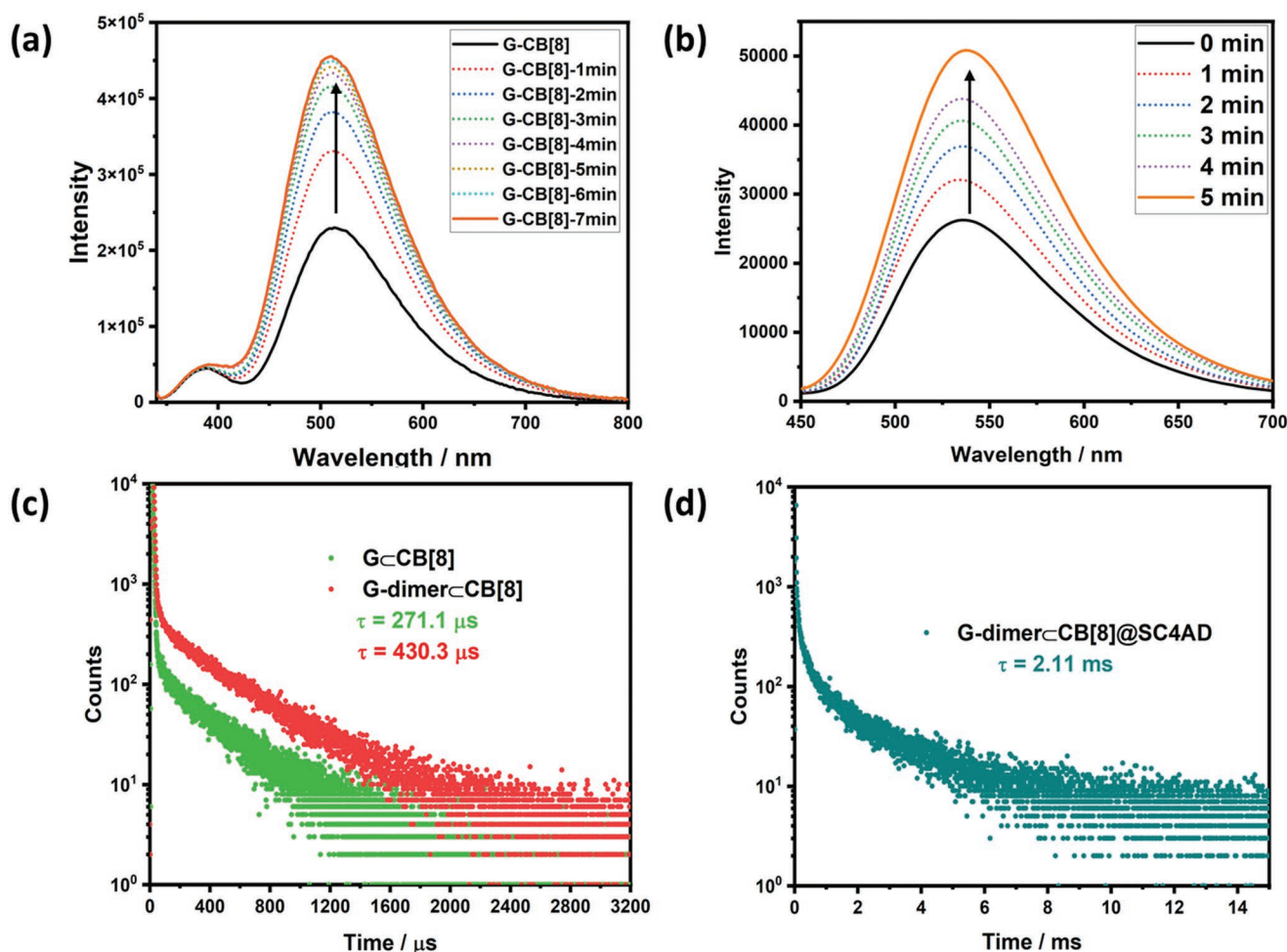
Figure 3. a) Phosphorescence spectra (delayed 0.1 ms) and b) AE/Φ_{ET} of G⊂CB[8]@SC4AD:RhB at different donor/acceptor ratios. c) Phosphorescence spectra (delayed 0.1 ms) and d) AE/Φ_{ET} of G-dimer⊂CB[8]@SC4AD:RhB at different donor/acceptor ratios. Time-resolved photoluminescence decay spectrum of e) G⊂CB[8]@SC4AD:RhB and f) G-dimer⊂CB[8]@SC4AD:RhB at 520 and 585 nm.

dimer (Figure 1d).[21] Importantly, the dimerization process of aggregate is almost quantitative in only about 4 min, while the single guest molecules do not form dimer even after irradiation at 365 nm for 1 h (Figure S25, Supporting Information), which also indicates that macrocyclic CB[8] can promote the dimer formation. In order to understand the inclusion mode of the assembly after illumination, 2D nuclear magnetic COSY

(Figure S26, Supporting Information) and ROESY (Figure S27, Supporting Information) were carried out. It can be found that there are clear correlations between pyridine salts themselves. Figure S28, Supporting Information, shows the TEM morphology comparison with different assembly forms. The guest molecule G self-assemblies to nano block after complexation with CB[8]. Upon further irradiation with UV light,

Figure 4. Effect of the irradiation of light of 365 nm. a) The steady state fluorescence emission spectra and b) phosphorescence spectra (delayed 0.1 ms) of G⊂CB[8] (λ_{ex} = 320 nm). Time-resolved photoluminescence decay spectrum of c) G⊂CB[8], G-dimer⊂CB[8], and d) G-dimer⊂CB[8]@SC4AD at 520 nm ([G] = [CB[8]] = 0.01 mM).

the coumarin group in G⊂CB[8] incurs photodimerization and transforms into nanowires (G-dimer⊂CB[8]). By measuring the UV absorption spectra of the system, it could be found that the maximum absorption with photodimerization is redshifted from 320 to 330 nm (Figure S29, Supporting Information). We held the view that the photodimerization of coumarin functional groups may narrow the intermolecular distance, leading to a better hydrophobic microenvironment and the increase of phosphorescence intensity and lifetime. When SC4AD was added to G-dimer⊂CB[8], we found that the phosphorescence intensity enhances (Figure S30, Supporting Information) and the life-time goes significantly from 430.3 μs to 2.11 ms.

Next, we consider the system formed by photodimerization of guest molecules (G-dimer⊂CB[8]@SC4AD) as the donor of energy transfer, and study the difference with the previous one. As exhibited in Figure 3c, the emission peak of G-dimer⊂CB[8]@SC4AD kept decreasing, and a new emission peak appeared at 585 nm and kept rising, which was the same as we mentioned above. However, the system irradiated by UV light shows higher energy Φ_{ET} and AE when energy transfer occurred. The Φ_{ET} of the light harvest system constructed

newly increased to 72.3% (Figure S31, Supporting Information). Accordingly, the maximum antenna effect value could reach 396.8 (Figure S34, Supporting Information, and Figure 3d), indicating that the light-regulated donor system has better energy transfer effect. In addition, the lifetime experiments show that the lifetimes at 520 and 585 nm were τ_1 = 237.1 μs and τ_2 = 381.1 μs, respectively (Figure 3f). We suspect that the reason why the system after photodimerization has better energy transfer effect is that the photodimerization of coumarin functional groups effectively enlarged the size of pseudorotaxane, which was conducive to the formation of larger size nanoparticles with SC4AD, thus contributing to dye loading and promoting energy transfer. As shown in Figure S28, Supporting Information, after photodimerization the nanoblocks with a few tens nanometers length changed to nanofibers with a micron orders length. Further secondary assembly with SC4AD, G-dimer⊂CB[8] formed larger nanoparticles compared to G⊂CB[8]. In addition, we have performed the experiments and calculated the loading content[22] of two nanoparticles (G⊂CB[8]@SC4AD and G-dimer⊂CB[8]@SC4AD) on RhB. The results showed that the loading content of G⊂CB[8]@SC4AD

on RhB was 27.8%, and that of G-dimer⊂CB[8]@SC4AD was 39.3%, which well supported our conclusion (Figures S37 and S38, Supporting Information).

Considering the higher Φ_{ET} of the dimerization (G-dimer⊂CB[8]@SC4AD:RhB), we utilized it as a donor to transfer energy to longer wavelength NIR dyes to achieve a cascade phosphorescent light capture system. Nile blue (NiB) and

Cy5 are two dyes that emit in the NIR region and their absorption had great spectral overlap with the emission of aggregate G-dimer⊂CB[8]@SC4AD:RhB (**Figure 5**a,b). As a result, they are selected as acceptors for secondary energy transfer. It could be observed that when NiB was added to G-dimer⊂CB[8]@SC4AD:RhB, the emission peak at 585 nm weakens gradually while a new emission peak at 680 nm appears and increases
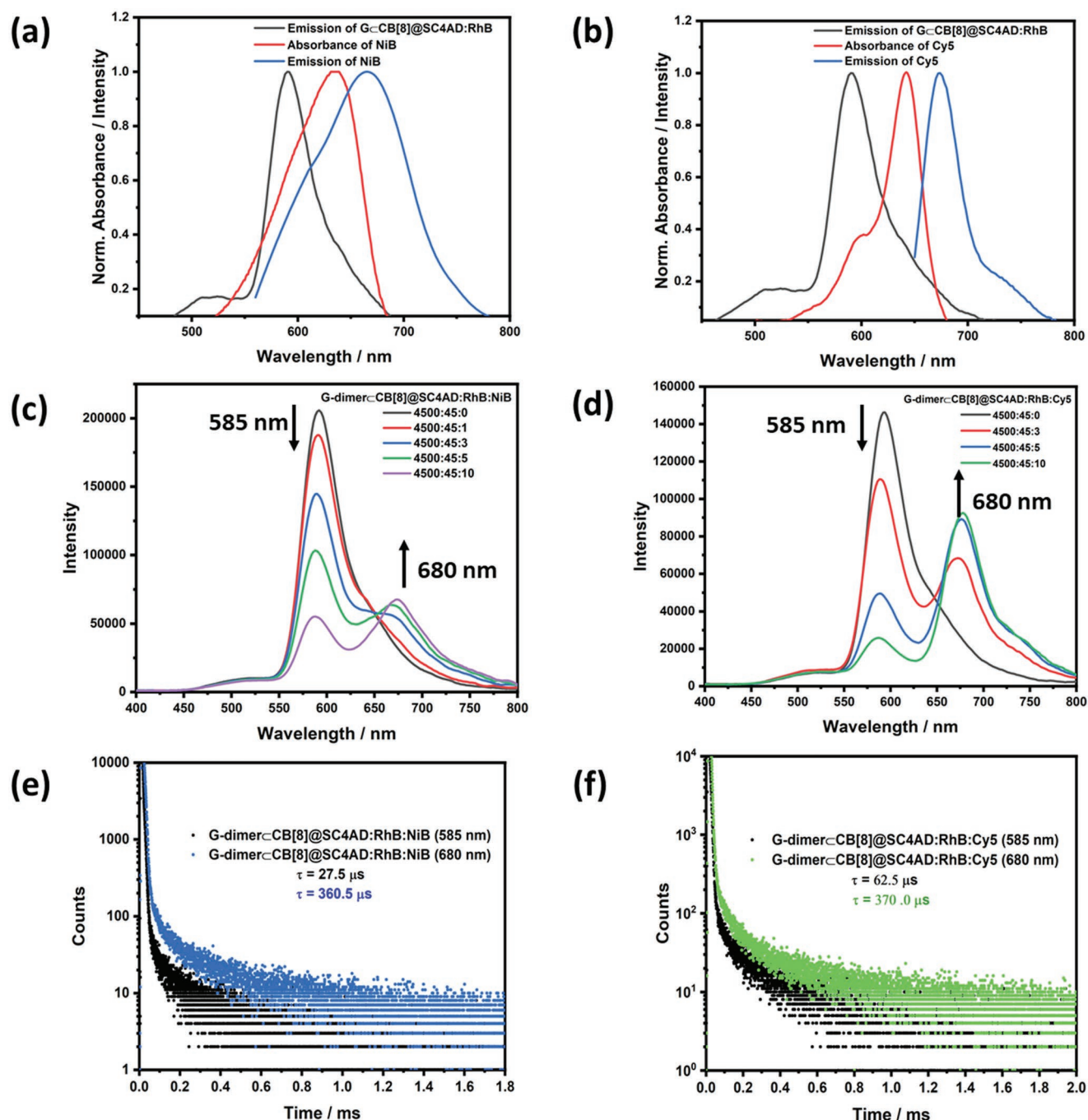
Figure 5. a) Normalized emission spectrum of G-dimer⊂CB[8]@SC4AD:RhB and absorption spectrum and emission spectrum of NiB. b) Absorption spectrum and emission spectrum of Cy5. Phosphorescence spectra (delayed 0.1 ms) of c) G-dimer⊂CB[8]@SC4AD:RhB:NiB and d) G-dimer⊂CB[8]@SC4AD:RhB:Cy5 at different donor/acceptor ratios. Time-resolved photoluminescence decay spectrum of e) G-dimer⊂CB[8]@SC4AD:RhB:NiB and f) G-dimer⊂CB[8]@SC4AD:RhB:Cy5 at 585 and 680 nm.
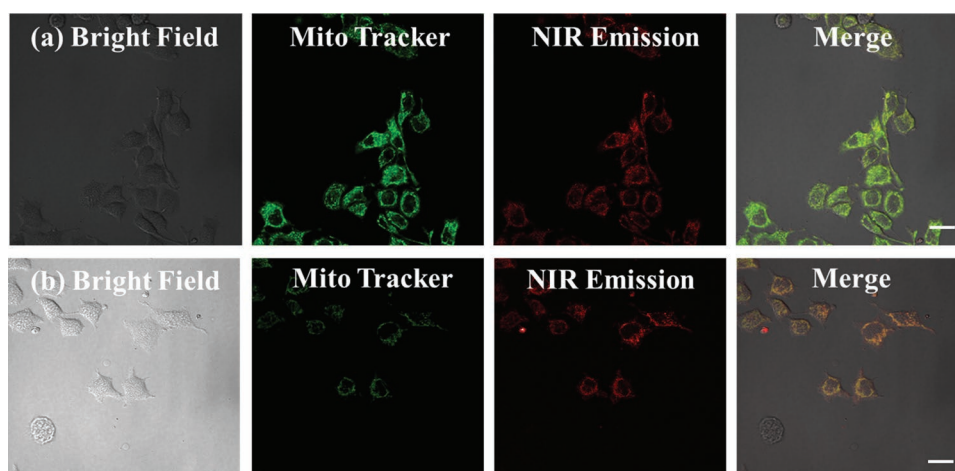
Figure 6. Confocal microscopy images of HeLa cells co-stained with a) G-dimer⊂CB[8]@SC4AD:RhB:NiB and b) G-dimer⊂CB[8]@SC4AD:RhB:Cy5 for MitoTracker Green, respectively. For MitoTracker Green, $\lambda_{ex} = 488$ nm and $\lambda_{em} = 500$–550 nm. For G-dimer⊂CB[8]@SC4AD:RhB:NiB and G-dimer⊂CB[8]@SC4AD:RhB:Cy5 (NIR emission), $\lambda_{ex} = 405$ nm and $\lambda_{em} = 650$–700 nm. Scale bar: 10 μm.

(Figure 5c). Importantly, the intensity of G-dimer⊂CB[8]@SC4AD at 520 nm remains almost constant, suggesting that the energy captured by the acceptors NiB is not transferred from there. The analysis of possible reasons mainly included the following two aspects: in the process of first-order energy transfer, the energy transfer efficiency was so high that the energy of the original donor has already been greatly quenched; furthermore, the spectral overlap of G-dimer⊂CB[8]@SC4AD and NiB was far less than that of RhB. As demonstrated in Figure 5e, the lifetime of 585 nm was measured to be 27.5 μs, while that of NiB at 680 nm was 360.5 μs. However, the lifetime of NiB alone stayed only in nano-second level, indicating the delayed fluorescence characteristics of NiB in the light capture system. The maximum Φ_{ET} and AE of the secondary energy transfer system were 90.66% (Figure S32, Supporting Information) and 213.85 (Figure S35, Supporting Information), respectively. Similarly, as Cy5 met the spectral conditions for secondary PET for G-dimer⊂CB[8]@SC4AD:RhB system, it was also identified as another acceptor (Figure 5b). As depicted in Figure 5d, in the process of adding Cy5 into the system, the absorption peak at 585 nm gradually decreased, and a new emission peak appeared at 680 nm. The original emission peak of G-dimer⊂CB[8]@SC4AD at 520 nm barely changed, indicating that the energy was transferred from the first-order system to Cy5, which also proved that Cy5 could be a qualified secondary acceptor of the system. In light of the lifetime experiments, the lifetime at 585 nm was reduced to 62.5 μs, while that at 680 nm was calculated as 370.0 μs, which conformed to the rule of delayed fluorescence (Figure 5f). When the mole ratio of G-dimer⊂CB[8]@SC4AD, RhB, and Cy5 reached 4500:45:10, Φ_{ET} was 82.34% (Figure S33, Supporting Information) and AE reached 232.79 (Figure S36, Supporting Information). In addition, it was worth explaining that the long life of 33.1 ms can be obtained after doping G-dimer⊂CB[8] into PVA (Figure S39, Supporting Information).

Based on the splendid phosphorescent-capture capability of the G-dimer⊂CB[8], we studied its application in living cell imaging. Human breast cancer cells (HeLa cells) were selected to complete the cytotoxicity test. After the cells were cultured

in medium containing G-dimer⊂CB[8]@SC4AD:RhB:NiB and G-dimer⊂CB[8]@SC4AD:RhB:Cy5 for a period of time, cell counting kit-8 was added to evaluate the toxicity of the cells. We noticed that even though the concentration of sample reached 50 μM and cultured in the incubator for 24 h, its toxic effect on the cells could still be ignored (Figure S40, Supporting Information). Subsequently, we carried out experiments with confocal laser scanning microscopy to investigate its biocompatibility and organelle localization characteristics. Assembly G-dimer⊂CB[8]@SC4AD:RhB:NiB was added to cell culture medium and continued to culture under this condition for 12 h, bright red luminescence was observed when the system was excited by a 408 nm laser (**Figure 6**). The above data together proved the successful PET from G-dimer⊂CB[8]@SC4AD to RhB and NiB successively, which enabled biological imaging in living cells. There was a good coincidence between the red luminous region and the green mitochondrial localization agent, and the Pearson colocalization coefficient reached 0.89, which proved that the light capture system has the property of targeting mitochondria (Figure S41, Supporting Information). The same operation was performed on G-dimer⊂CB[8]@SC4AD:RhB:Cy5, and beyond all doubt, the result was consistent with what we mentioned above.

3. Conclusion

In summary, we constructed a supramolecular biaxial polypseudorotaxane by the guest molecule G and CB[8] to obtain purely organic RTP. And then, the amphiphilic calixarene SC4AD was added to further enhance the phosphorescence intensity, achieving an extremely long-lifetime (2.89 ms) phosphorescence in aqueous solution. Interestingly, the photodimerization of coumarin functional group in the guest molecule occurred after the system was irradiated by UV light, which resulted in a significant increasement of phosphorescence intensity, specifically, the quantum yield increased from 5.1% to 25.7%. Based on the good luminescence properties of the above systems, we used them as energy donors to construct phosphorescent

energy transfer systems. It was worth noting that the photodimerization system has better energy transfer effect under the same conditions. As a result, it was selected as target donor to construct cascade phosphorescent capturer to obtain delayed NIR fluorescence. Moreover, it has been successfully applied to mitochondrial targeting cell imaging due to the low toxicity of the system. This multi-charged supramolecular assembly is expected to afford a well-suited and viable strategy for long-lifetime PL of cascaded phosphorescent energy transfer system.

Supporting Information

Supporting Information is available from the Wiley Online Library or from the author.

Conflict of Interest

The authors declare no conflict of interest.

Data Availability Statement

The data that support the findings of this study are available from the corresponding author upon reasonable request.

[1] a) X. Ma, J. Wang, H. Tian, *Acc. Chem. Res.* **2019**, *52*, 738; b) Q. Peng, H. Ma, Z. Shuai, *Acc. Chem. Res.* **2021**, *54*, 940; c) Z. Y. Zhang, Y. Liu, *Chem. Sci.* **2019**, *10*, 7773.

[2] a) J. Yang, X. Wu, J. Shi, B. Tong, Y. Lei, Z. Cai, Y. Dong, *Adv. Funct. Mater.* **2021**, *31*, 2108072; b) S. Kuila, S. J. George, *Angew. Chem., Int. Ed.* **2020**, *59*, 9393; c) W. Zhao, T. S. Cheung, N. Jiang, W. Huang, J. W. Y. Lam, X. Zhang, Z. He, B. Z. Tang, *Nat. Commun.* **2019**, *10*, 1595; d) M. Huo, X. Y. Dai, Y. Liu, *Small* **2022**, *18*, e2104514; e) F. F. Shen, Y. Chen, X. Dai, H. Y. Zhang, B. Zhang, Y. Liu, Y. Liu, *Chem. Sci.* **2020**, *12*, 1851; f) W. W. Xu, Y. Chen, Y. L. Lu, Y. X. Qin, H. Zhang, X. Xu, Y. Liu, *Angew. Chem., Int. Ed.* **2022**, *61*, e202115265.

[3] J. Yu, H. Wang, Y. Liu, *Adv. Opt. Mater.* **2022**, *10*, 2201761.

[4] a) L. Bian, H. Shi, X. Wang, K. Ling, H. Ma, M. Li, Z. Cheng, C. Ma, S. Cai, Q. Wu, N. Gan, X. Xu, Z. An, W. Huang, *J. Am. Chem. Soc.* **2018**, *140*, 10734; b) X. Zhang, Y. Cheng, J. You, J. Zhang, Y. Wang,

J. Zhang, *ACS Appl Mater Interfaces* **2022**, *14*, 16582; c) S. Cai, H. Shi, D. Tian, H. Ma, Z. Cheng, Q. Wu, M. Gu, L. Huang, Z. An, Q. Peng, W. Huang, *Adv. Funct. Mater.* **2018**, *28*, 1705045; d) X. Yao, J. Wang, D. Jiao, Z. Huang, O. Mhirsi, F. Lossada, L. Chen, B. Haehnle, A. J. C. Kuehne, X. Ma, H. Tian, A. Walther, *Adv. Mater.* **2021**, *33*, 2005973; e) K. Jiang, L. Zhang, J. Lu, C. Xu, C. Cai, H. Lin, *Angew. Chem., Int. Ed.* **2016**, *55*, 7231; f) J. Zhang, S. Xu, Z. Wang, P. Xue, W. Wang, L. Zhang, Y. Shi, W. Huang, R. Chen, *Angew. Chem., Int. Ed.* **2021**, *60*, 17094; g) H.-J. Wang, W.-W. Xing, Z.-H. Yu, H.-Y. Zhang, W.-W. Xu, Y. Liu, *Adv. Opt. Mater.* **2022**, *10*, 2201903; h) Q. Wang, Z. Qi, Q. M. Wang, M. Chen, B. Lin, D. H. Qu, *Adv. Funct. Mater.* **2022**, *32*, 2208865; i) Z. Zong, Q. Zhang, S. H. Qiu, Q. Wang, C. Zhao, C. X. Zhao, H. Tian, D. H. Qu, *Angew. Chem., Int. Ed.* **2022**, *61*, e202116414. j) Q. Wang, Q. Zhang, Q. W. Zhang, X. Li, C. X. Zhao, T. Y. Xu, D. H. Qu, H. Tian, *Nat. Commun.* **2020**, *11*, 158; k) Q. Wang, B. Lin, M. Chen, C. Zhao, H. Tian, D. H. Qu, *Nat. Commun.* **2022**, *13*, 4185.

[5] a) X. Zhen, Y. Tao, Z. An, P. Chen, C. Xu, R. Chen, W. Huang, K. Pu, *Adv. Mater.* **2017**, *29*, 1606665; b) X. Y. Dai, X. Huo, X. Dong, Y. Y. Hu, Y. Liu, *Adv. Mater.* **2022**, *34*, 2203534; c) X. F. Wang, H. Xiao, P. Z. Chen, Q. Z. Yang, B. Chen, C. H. Tung, Y. Z. Chen, L. Z. Wu, *J. Am. Chem. Soc.* **2019**, *141*, 5045; d) X. Cao, S. R. Allu, S. Jiang, M. Jia, J. R. Gunn, C. Yao, E. P. LaRochelle, J. R. Shell, P. Bruza, D. J. Gladstone, L. A. Jarvis, J. Tian, S. A. Vinogradov, B. W. Pogue, *Nat. Commun.* **2020**, *11*, 573; e) X. K. Ma, Y. M. Zhang, Q. Yu, H. Zhang, Z. Zhang, Y. Liu, *Chem. Commun.* **2021**, *57*, 1214.

[6] a) X. Y. Dai, Y. Y. Hu, Y. Sun, M. Huo, X. Dong, Y. Liu, *Adv. Sci.* **2022**, *9*, 2200524; b) T. Zhang, X. Ma, H. Wu, L. Zhu, Y. Zhao, H. Tian, *Angew. Chem., Int. Ed.* **2020**, *59*, 11206; c) H. Zhu, I. Badia-Dominguez, B. Shi, Q. Li, P. Wei, H. Xing, M. C. R. Delgado, F. Huang, *J. Am. Chem. Soc.* **2021**, *143*, 2164; d) Y.-C. Liang, S.-S. Gou, K.-K. Liu, W.-J. Wu, C.-Z. Guo, S.-Y. Lu, J.-H. Zang, X.-Y. Wu, Q. Lou, L. Dong, Y.-F. Gao, C.-X. Shan, *Nano Today* **2020**, *34*, 100900; e) T. Su, Y.-H. Liu, Y. Chen, Y. Liu, *J. Mater. Chem. C* **2022**, *10*, 2623.

[7] a) D. Lee, O. Bolton, B. C. Kim, J. H. Youk, S. Takayama, J. Kim, *J. Am. Chem. Soc.* **2013**, *135*, 6325; b) W. L. Zhou, W. Lin, Y. Chen, X. Y. Dai, Z. Liu, Y. Liu, *Chem. Sci.* **2022**, *13*, 573.

[8] a) Y. Gong, G. Chen, Q. Peng, W. Z. Yuan, Y. Xie, S. Li, Y. Zhang, B. Z. Tang, *Adv. Mater.* **2015**, *27*, 6195; b) S. Garain, S. M. Wagalgave, A. A. Kongasseri, B. C. Garain, S. N. Ansari, G. Sardar, D. Kabra, S. K. Pati, S. J. George, *J. Am. Chem. Soc.* **2022**, *144*, 10854; c) J. Yang, X. Zhen, B. Wang, X. Gao, Z. Ren, J. Wang, Y. Xie, J. Li, Q. Peng, K. Pu, Z. Li, *Nat. Commun.* **2018**, *9*, 840.

[9] a) Y. Su, Y. Zhang, Z. Wang, W. Gao, P. Jia, D. Zhang, C. Yang, Y. Li, Y. Zhao, *Angew. Chem., Int. Ed.* **2020**, *59*, 9967; b) Z. Y. Zhang, W. W. Xu, W. S. Xu, J. Niu, X. H. Sun, Y. Liu, *Angew. Chem., Int. Ed.* **2020**, *59*, 18748; c) L. Gu, H. Wu, H. Ma, W. Ye, W. Jia, H. Wang, H. Chen, N. Zhang, D. Wang, C. Qian, Z. An, W. Huang, Y. Zhao, *Nat. Commun.* **2020**, *11*, 944.

[10] a) S. Kuila, S. Garain, S. Bandi, S. J. George, *Adv. Funct. Mater.* **2020**, *30*, 2003693; b) M. Louis, H. Thomas, M. Gmelch, A. Haft, F. Fries, S. Reineke, *Adv. Mater.* **2019**, *31*, 1807887; c) Z. A. Yan, X. Lin, S. Sun, X. Ma, H. Tian, *Angew. Chem., Int. Ed.* **2021**, *60*, 19735.

[11] a) X. Yu, W. Liang, Q. Huang, W. Wu, J. J. Chruma, C. Yang, *Chem. Commun.* **2019**, *55*, 3156; b) P. Wei, X. Zhang, J. Liu, G. G. Shan, H. Zhang, J. Qi, W. Zhao, H. H. Sung, I. D. Williams, J. W. Y. Lam, B. Z. Tang, *Angew. Chem., Int. Ed.* **2020**, *59*, 9293; c) Y. Lei, W. Dai, J. Guan, S. Guo, F. Ren, Y. Zhou, J. Shi, B. Tong, Z. Cai, J. Zheng, Y. Dong, *Angew. Chem., Int. Ed.* **2020**, *59*, 16054; d) W. L. Zhou, Y. Chen, Q. Yu, H. Zhang, Z. X. Liu, X. Y. Dai, J. J. Li, Y. Liu, *Nat. Commun.* **2020**, *11*, 4655.

[12] X. K. Ma, Y. Liu, *Acc. Chem. Res.* **2021**, *54*, 3403.

[13] a) C. Xu, C. Yin, W. Wu, X. Ma, *Chem* **2021**, *65*, 75; b) C. Wang, X. K. Ma, P. Guo, C. Jiang, Y. H. Liu, G. Liu, X. Xu, Y. Liu, *Adv. Sci.*

**ADVANCED
SCIENCE NEWS**

www.advancedsciencenews.com

**ADVANCED
OPTICAL
MATERIALS**

www.advopticalmat.de

2022, *9*, 2103041; c) Z. Wang, T. Li, B. Ding, X. Ma, *Chin. Chem. Lett.* **2020**, *31*, 2929; d) T. Li, X. Ma, *Dyes Pigm.* **2018**, *148*, 306.

[14] S. Garain, B. C. Garain, M. Eswaramoorthy, S. K. Pati, S. J. George, *Angew. Chem., Int. Ed.* **2021**, *60*, 19720.

[15] M. Huo, X. Y. Dai, Y. Liu, *Angew. Chem., Int. Ed.* **2021**, *60*, 27171.

[16] H. J. Yu, Q. Zhou, X. Dai, F. F. Shen, Y. M. Zhang, X. Xu, Y. Liu, *J. Am. Chem. Soc.* **2021**, *143*, 13887.

[17] a) S. R. Trenor, A. R. Shultz, B. J. Love, T. E. Long, *Chem. Rev.* **2004**, *104*, 3059; b) D. Cao, Z. Liu, P. Verwilst, S. Koo, P. Jangjili, J. S. Kim, W. Lin, *Chem. Rev.* **2019**, *119*, 10403.

[18] a) Z. Y. Zhang, Y. Chen, Y. Liu, *Angew. Chem., Int. Ed.* **2019**, *58*, 6028; b) X. K. Ma, W. Zhang, Z. Liu, H. Zhang, B. Zhang, Y. Liu, *Adv. Mater.* **2021**, *33*, 2007476.

[19] H. Nie, Z. Wei, X. L. Ni, Y. Liu, *Chem. Rev.* **2022**, *122*, 9032;

[20] X. M. Chen, Y. Chen, Q. Yu, B. H. Gu, Y. Liu, *Angew. Chem., Int. Ed.* **2018**, *57*, 12519.

[21] H.-J. Wang, H.-Y. Zhang, W.-W. Xing, H. Wu, Y.-L. Cui, Y. Liu, *Chin. Chem. Lett.* **2022**, *33*, 4033.

[22] Z.-Y. Li, Y. Chen, H. Wu, Y. Liu, *ChemistrySelect* **2018**, *3*, 3203.